Scilight

Nano-electrochemistry & Nano-photochemistry

https://www.sciltp.com/journals/nenp

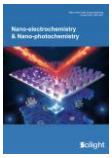

Article

Surface-Enhanced Raman Scattering Platform Based on ZnO@ZIF-8 Composite for the Detection of Periodontal Pathogens

Xinyi Zhang [1], Zhenhuan Liu [1], Qing Liu [1], Xuan Xu [2] and Tingting Zheng [1,*]

[1] Shanghai Key Laboratory of Green Chemistry and Chemical Processes, Department of Chemistry, School of Chemistry and Molecular Engineering, East China Normal University, Shanghai 200241, China

[2] State Key Laboratory of Analytical Chemistry for Life Science, School of Chemistry and Chemical Engineering, Nanjing University, Nanjing 210093, China

* Correspondence: ttzheng@chem.ecnu.edu.cn

How To Cite: Zhang, X.; Liu, Z.; Liu, Q.; et al. Surface-Enhanced Raman Scattering Platform Based on ZnO@ZIF-8 Composite for the Detection of Periodontal Pathogens. *Nano-electrochemistry & Nano-photochemistry* **2025**, *1*(1), 5. https://doi.org/10.53941/nenp.2025.100005.

Received: 30 September 2025
Revised: 30 October 2025
Accepted: 7 November 2025
Published: 13 November 2025

Abstract: Periodontitis, which owns a significant prevalence rate, is a chronic inflammatory disorder caused by the infection of multiple microorganisms. *Porphyromonas gingivalis* (*P. gingivalis*) serves as a key pathogenic biomarker for periodontitis. However, currently, there is a lack of diagnostic tools that are able to quickly and precisely quantify levels of *P. gingivalis*. Therefore, developing a quantitative detection method for this pathogenic bacterium is critical for the diagnosis and management of this disease. Herein, based on the petal-like spherical ZnO@ZIF-8 composite substrate, we built an innovative semiconductor surface-enhanced Raman spectroscopic (SERS) platform specifically engineered for the detection of *P. gingivalis* with high speed, sensitivity, and stability. The detection of *P. gingivalis* on this SERS platform takes only 30 min. It also has excellent long-term stability for over 60 days. This platform exhibits an extensive linear range from 4×10^3 CFU/mL to 4×10^8 CFU/mL, while also owning a low limit of detection (LOD) of 38 CFU/mL for *P. gingivalis*. The developed method provides a novel pathway for precise diagnosis and efficient screening of periodontitis, and explores new directions for detecting other disease-related biomolecules, including proteins, small molecules, peptides, and miRNAs at the same time.

Keywords: zinc oxide; *Porphyromonas gingivalis*; semiconductor; bacterial detection; electromagnetic enhancement

1. Introduction

Periodontitis (CP), also known as destructive gum disease, is one of the six most common non-communicable diseases worldwide [1–3]. Periodontitis is characterized by progressive destruction of periodontal tissues, manifested primarily as loss of connective tissue attachment and alveolar bone resorption, which may ultimately lead to increased tooth mobility or even tooth loss [4]. Severe periodontitis affects approximately 19% of the global population aged 15 years and above [5], exhibiting high prevalence, particularly among elderly populations [6,7]. *P. gingivalis* is recognized as the primary pathogenic microorganism driving periodontitis. Traditional culture methods, as well as the polymerase chain reaction (PCR) technique, are widely seen in the laboratory [8,9]. Nonetheless, traditional culture methods are time-consuming and exhibit limited sensitivity, while PCR is prone to having high costs and limiting its clinical applicability due to cumbersome operations [10–12].

In contrast, Surface-enhanced Raman spectroscopy (SERS) technology is regarded as a promising analytical method that provides various molecules absorbed with their ample vibrational spectroscopic information [13–15]. This approach has been effectively utilized for the characterization and quantification of various substances,

encompassing chemicals, metabolites, macromolecules, and microorganisms [16,17]. Additionally, over recent years, the employment of semiconductor materials as SERS substrates has gained growing prevalence, due to not only their notable stability, but also their biocompatibility and unique photometric characteristics [18,19].

Herein, based on the petal-like spherical ZnO@ZIF-8 semiconductor composite, we developed a SERS platform for rapid, ultra-sensitive, and stable detection of periodontal pathogenic microorganisms. Additionally, the para-nitrophenol (pNTP) molecule was employed to verify the electromagnetic enhancement of the SERS substrate. After that, we built the SERS platform. 4-cyanobenzoic acid was introduced as a signal molecule, with its characteristic fingerprint peak located in the "Raman biological silent zone" (1800–2800 cm^{-1}) [20,21], where interference from proteins, ions, and other substances is negligible—enabling highly specific detection of low-concentration *P. gingivalis*. This platform successfully achieved sensitive and rapid detection with a LOD of 38 CFU/mL in approximately 30 min, and had a favorable stability for around 60 days. This work provides a promising novel technology platform for the SERS assay in the detection of *P. gingivalis*.

2. Materials and Methods

2.1. Chemicals and Instruments

All chemical reagents we used were purchased from commercial reagent suppliers and were employed directly without further purification. Detailed information regarding employed chemicals and instruments is provided in the Supplementary Materials (Tables S1 and S2).

2.2. Synthesis of ZnO Nanoparticles

In brief, 0.01 mol of $Zn(CH_3COO)_2 \cdot 2H_2O$ was first added to 100 mL of DEG in a glass flask. The mixture was then heated to 160 °C slowly and kept at 160 °C under magnetic stirring for 1 h for the formation of a cloudy colloidal suspension. Then, the colloidal suspension was cooled down to room temperature and centrifuged at 12,000 rpm for 5 min. The sediment was discarded, and the supernatant was used as a seed solution for further reactions. In a separate glass flask, another 0.01 mol of $Zn(CH_3COO)_2 \cdot 2H_2O$ was dissolved in 100 mL of DEG. The temperature of the mixture solution was slowly raised to 130 °C, followed immediately by the addition of 0.3 mL of seed solution. After that, the temperature was raised to 160 °C promptly. We then kept this mixture at the same temperature under magnetic stirring for 1 h for the formation of spherical ZnO nanoparticles. ZnO nanoparticles were then collected by centrifugation, followed by washing with distilled water and anhydrous ethanol several times. Afterwards, ZnO nanoparticles were dried at 60 °C for 12 h in a vacuum drier before use.

2.3. Synthesis of ZnO@ZIF-8 Nanoparticles

A total of 0.0204 g of as-synthesized ZnO nanoparticles was first added to 16 mL of DMF/H_2O (10:1 in volume ratio) solution dissolved with 0.11 g of 2-methylimidazole. The mixture was ultrasonicated for 10 min to disperse ZnO nanoparticles. After that, the mixture was transferred to an oil bath, which was preheated to 70 °C. ZnO@ZIF-8 nanoparticles were formed after reacting at 70 °C for 3 h. They were collected by centrifugation and washed with DMF and ethanol several times. After that, ZnO@ZIF-8 nanoparticles were dried at 60 °C for 12 h in a vacuum drier before use.

2.4. pNTP Detection (Liquid Phase) on ZnO@ZIF-8 Nanoparticles

ZnO@ZIF-8 composite weighing 5 mg was dispersed in 5 mL of pNTP solution (ethanol) of a certain concentration. The mixture was incubated for 2 h. ZnO@ZIF-8 nanoparticles were then collected by centrifuge and transferred onto the stage of the Raman microscope for direct SERS measurement.

2.5. Synthesis of Amino-Modified ZnO@ZIF-8

An appropriate number of ZnO@ZIF-8 nanoparticles were added to 5 mL of ethanol solution containing 2 mL of APTES and gently shaken for 6 h. After the reaction was completed, centrifuge with anhydrous ethanol, wash 2–3 times, and finally freeze-dry for 12 h.

2.6. Construction and Detection of the SERS Platform for P. gingivalis

First, dissolve 5 mg of amino-functionalized ZnO@ZIF-8 in 3 mL of ultrapure water, and while stirring, add 30 μL of the aptamer. Stir for 1 h to obtain solution A. Meanwhile, dissolve 10 mg of 4-cyano-benzoic acid in 3 mL of ultrapure water, and while stirring, add 30 μL of cDNA. Stir for 1 h to get solution B. Mix solution A with

solution B, and stir for 2 h to obtain solution C, washing with 0.01 M PBS solution. The SERS platform has been successfully established. Add a sample of *P. gingivalis*. The cell concentration of the *P. gingivalis* culture was evaluated by measuring the optical density at 600 nm (OD_{600}), and the measured value was 0.403. Based on the reported concentration conversion standard for *P. gingivalis* (i.e., an OD_{600} of 0.1 corresponds to approximately 1×10^8 CFU/mL), the viable cell concentration of the culture was calculated to be 4×10^8 CFU/mL. To establish a series of concentration gradients, the aforementioned bacterial suspension was subjected to serial gradient dilution, resulting in 6 groups of bacterial suspensions with 6 different concentrations (from 4×10^3 CFU/mL to 4×10^8 CFU/mL) in decreasing order of concentration. All diluted bacterial suspensions were placed in a constant-temperature stirring device and continuously stirred for 2 h.

2.7. Detection of the SERS Platform for P. gingivalis (in Artificial Saliva Solution)

A total of 3 mL of solution C from the aforementioned concentration gradient system was pipetted and mixed thoroughly with 3 mL of artificial saliva. Add a sample of *P. gingivalis*. After uniform oscillation of the mixed system, the optical density at 600 nm (OD_{600}) was measured using a UV-visible spectrophotometer, yielding a result of 0.367. To further establish a multi-concentration analysis model, the mixed solution was subjected to systematic gradient dilution, sequentially preparing 6 groups of *P. gingivalis* suspensions with different concentrations (from 4×10^3 CFU/mL to 4×10^8 CFU/mL), decreasing in order. All diluted bacterial suspensions were placed in a constant-temperature stirring device and continuously stirred for 2 h.

3. Results and Discussion

3.1. Synthesis and Characterization of ZnO@ZIF-8

The ZnO@ZIF-8 nanoparticles were prepared by the in-situ synthesis method [22]. Firstly, it could be seen from the scanning electron microscope (SEM) images (Supplementary Materials Figures S4 and S5) that the ZnO nanoparticles were spherical, and the entire nano-chain structure was composed of countless nano-spheres with an average diameter of 150–200 nm; ZIF-8 was hexagonal, with a diameter estimated around 200–250 nm. As shown in Figure 1A, ZnO@ZIF-8 nanoparticles were petal-shaped and spherical, with a diameter of approximately 450–750 nm. The entire nano-flower structure was composed of spherical ZnO with hexagonal ZIF-8 polymerized on the surface. Sharp edges representing ZIF-8 coated on the surfaces of ZnO@ZIF-8 nanoparticles enabled ZnO@ZIF-8 composite to be distinguished from their original ZnO cores. As presented in Figure 1C, the high-resolution TEM (HRTEM) image indicated that our ZnO@ZIF-8 nanoparticles synthesized in this work possessed favorable crystalline properties. A lattice spacing of 0.246 nm was observed, which was consistent with the nanostructures synthesized using a similar method in previous studies [22]. The energy dispersive spectrum (EDS) diagram demonstrated (Figure 1D) that ZnO@ZIF-8 comprised the elements Zn, C, N, and O. Uniform distribution was observed for carbon and nitrogen elements throughout the ZnO@ZIF-8 composite, while zinc as well as oxygen elements mainly concentrated in the core area. In the XRD spectrum (Figure 1E), the different diffraction peaks located at 7.48°, 10.52°, 12.86°, 14.84°, 16.58°, and 18.16° correspond respectively to the crystal planes (001), (002), (112), (022), (013), and (222) representing ZIF-8. The ZnO@ZIF-8 composite material shows three new peaks at 31.78°, 34.44°, and 36.34°, corresponding to the (100), (002), and (101) crystal planes of ZnO compared with pure ZIF-8 [23]. As shown in Figure 1F, Raman spectroscopy was conducted on ZIF-8, ZnO, and ZnO@ZIF-8. ZIF-8 exhibited distinct signal peaks at 686 cm^{-1}, 1023 cm^{-1}, 1147 cm^{-1}, 1189 cm^{-1}, 1462 cm^{-1} and 1508 cm^{-1}. Compared with pure ZIF-8, a new peak was observed at 990 cm^{-1} in the ZnO@ZIF-8 composite, and the same peak position was also found on ZnO, which confirmed the effective combination of the two. Additionally, in the FT-IR spectroscopy (Figure 1G), the main peaks representing ZnO and ZIF-8 were explicitly visible in the ZnO@ZIF-8 composite. The characteristic peaks of ZIF-8 were at 758 cm^{-1} and 1145 cm^{-1}, while those of ZnO were at 559 cm^{-1} and 3390 cm^{-1}. The ZnO@ZIF-8 composite after combination had both the peak of ZnO at 559 cm^{-1} and the peaks of ZIF-8 at 758 cm^{-1} and 1145 cm^{-1}. The strong absorption peak located in 3300–3500 cm^{-1} corresponded to the stretching vibration of the O-H group, and the strong FT-IR peak at 500–600 cm^{-1} was the result of the stretching vibration of the Zn-O bond [24,25]. The analysis from X-ray diffraction (XRD) is consistent with the results from scanning electron microscopy (SEM): both zinc oxide and ZIF-8 diffraction signals are present in the ZnO@ZIF-8 nanoparticles, indicating that some zinc oxide has been partially converted to ZIF-8. However, the X-ray photoelectron spectroscopy (XPS) spectrum only shows the characteristic signal of ZIF-8. Also, as illustrated in Figure 1B, the TEM image of ZnO@ZIF-8 explicitly demonstrated that the ZIF-8 shell layer has already covered the surface of the zinc oxide nanoparticles. Both suggested that the ZIF-8 shell has fully covered the surface of the zinc oxide [19,26].

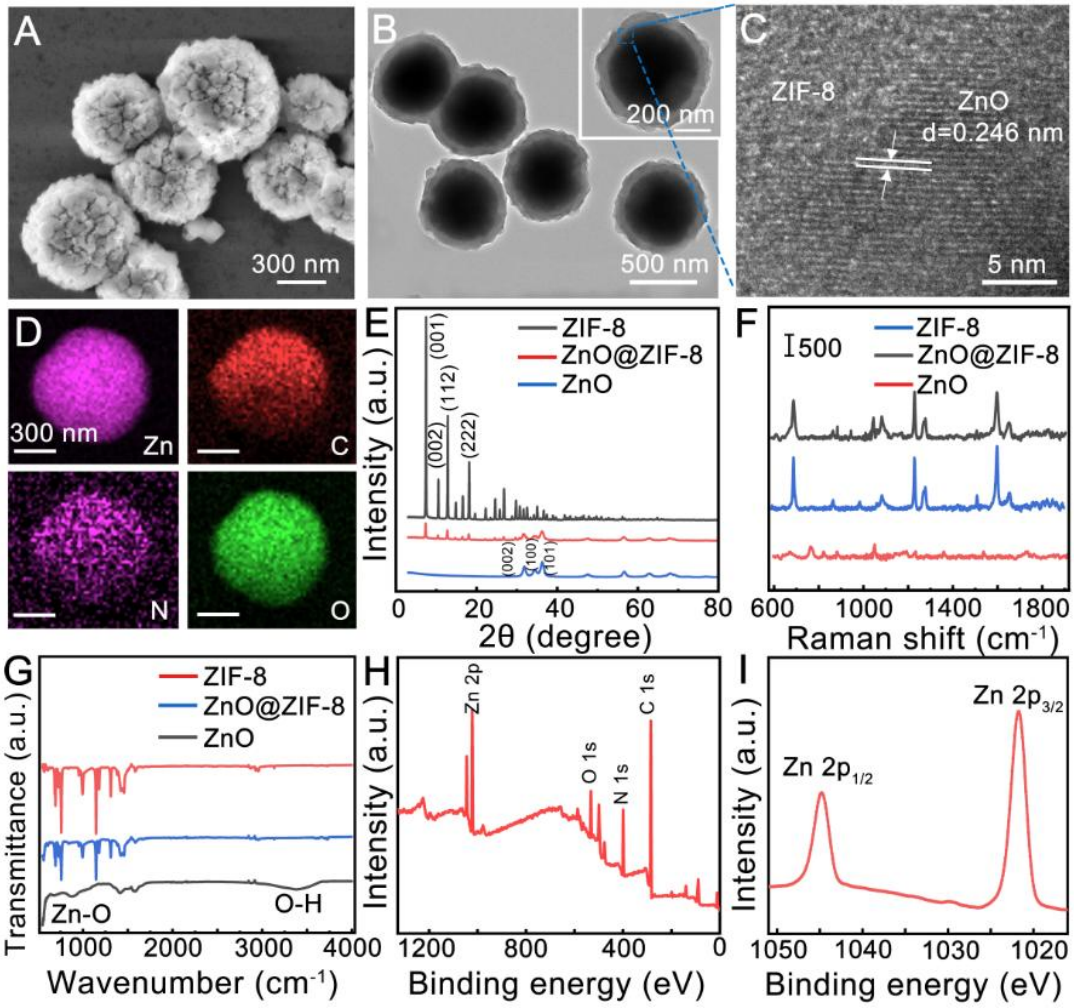

Figure 1. (**A**) SEM image of ZnO@ZIF-8; (**B**) TEM image of ZnO@ZIF-8; (**C**) HRTEM image of ZnO@ZIF-8; (**D**) EDS mapping of ZnO@ZIF-8; (**E**) XRD patterns; (**F**) Raman spectra; and (**G**) FTIR spectra of ZnO, ZIF-8, and ZnO@ZIF-8; (**H**) Survey XPS spectra of ZnO@ZIF-8; (**I**)Zn 2p XPS spectra of ZnO@ZIF-8.

3.2. Mechanism of Raman Enhancement in ZnO@ZIF-8

Para-nitrophenol (pNTP) is a chosen probe molecule with a strong adsorption thiol group. It is able to undergo chemical adsorption on the surface of ZnO, generating a chemical enhancement mechanism (CM) signal based on charge transfer resonance. By comparing the signal differences between CM and electromagnetic enhancement mechanism (EM), the contribution of EM can be clearly identified, making it perfect to study the mechanism of the SERS enhancement for ZnO@ZIF-8 composite [27,28]. As illustrated in Figure 2A, SERS peaks of pNTP at around 1326 cm^{-1} are detectable on both ZnO and ZnO@ZIF-8 nanoparticles, but cannot be observed when mixed with ZIF-8 nanoparticles, which demonstrates that the ZIF-8 shell does not possess SERS activity, while the SERS activity of ZnO@ZIF-8 composite mainly originates from the internal ZnO core. Different from the regular pNTP Raman peak shown at 1326 cm^{-1}, the peak witnessed on ZnO@ZIF-8 nanoparticles at 1339 cm^{-1}, representing pTNP, has marginally shifted, suggesting the enhancement of the Raman signal stems from the pNTP molecules and the ZnO core, considering the charge transfer resonance between them [29,30]. Based on this speculation, a series of concentrations of pNTP molecules on ZnO@ZIF-8 composite was designed. As shown in Figure 2B,C, the intensity of Raman peaks at 1326 cm^{-1} increased rapidly, while peaks at 1339 cm^{-1} basically remained still. Thus, it was supposed that the presence of a peak at 1326 cm^{-1} was attributed to the EM caused by the pNTP molecules, which were enriched on the ZIF-8 shell rather than directly attaching to the ZnO core. Figure 2D–F explained the EM as a result of the unique structure of ZnO@ZIF-8 composite. Firstly, when pTNP concentrations were relatively low, most pNTP molecules were capable of reaching the surface of ZnO core, generating a CM enhancement peak at 1339 cm^{-1}, while only a few of them were enriched on the ZIF-8 shell and generated weak Raman signal at 1326 cm^{-1}, which was formed by the affection of the ZnO core since its strong electromagnetic field generating around. As illustrated in Figure 2E, at low pNTP concentrations, the CM peak is slightly stronger than the EM peak. As the pNTP concentrations grew, the intensity of both EM and CM peaks rose until the pNTP

molecules were able to form a monolayer at the surface of the ZnO core. Subsequently, even if the pNTP concentrations continuously increased, the signal of the CM pNTP peak remained almost unchanged because the ZnO surface was not able to accommodate more pNTP molecules. In contrast, the intensity of the EM pNTP peak grew increasingly because the ZIF-8 shell still had space holding more pNTP molecules. Eventually, it led to the intensity of the electromagnetic enhancement peak being stronger than that of its chemical enhancement peak, indicating that above the monolayer coverage concentration, the number of pNTP molecules captured by the ZIF-8 shell might exceed those adsorbed on the ZnO core (Figure 2F).

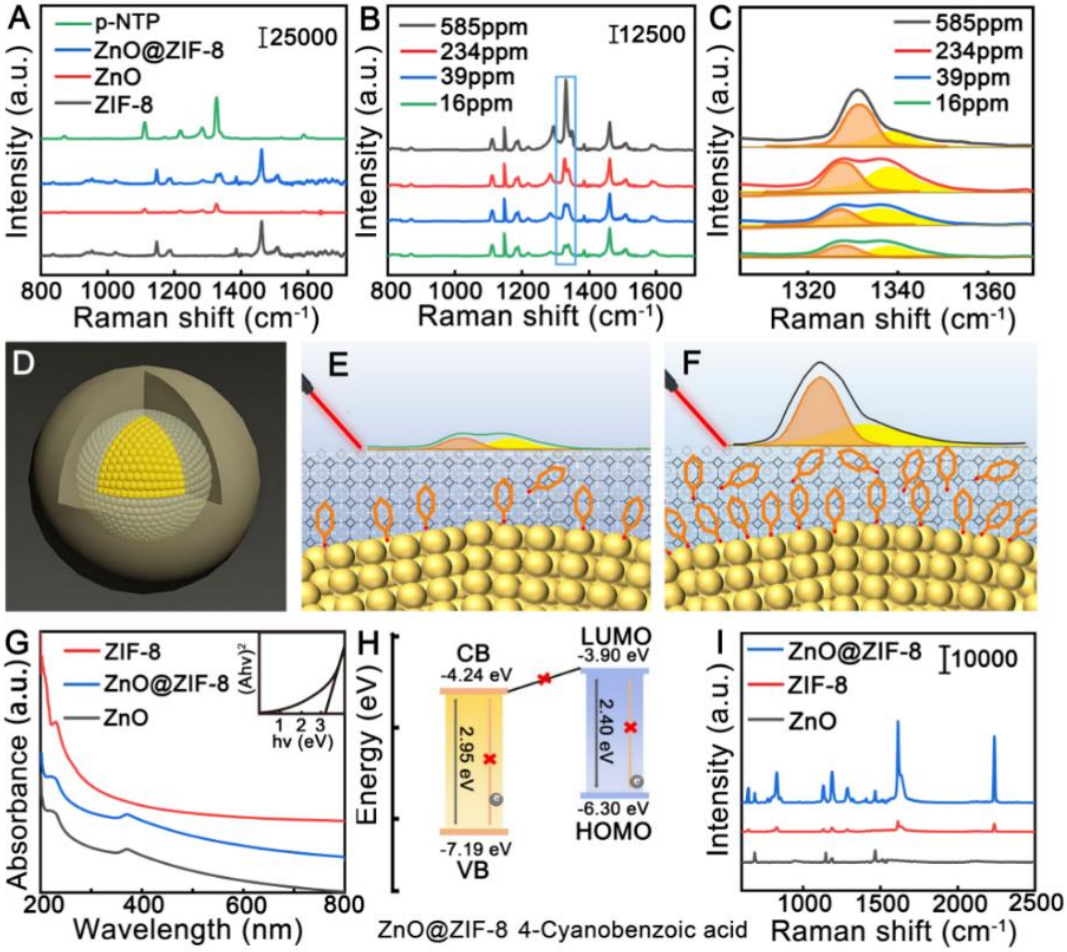

Figure 2. (**A**) Raman spectra of pNTP molecules (green) on ZIF-8 (black), ZnO (red), and ZnO@ZIF-8 (blue) nanoparticles used as SERS substrates; (**B**) SERS spectra of pNTP with a series of concentration acquired by using ZnO@ZIF-8 nanoparticles as enhancing materials; (**C**) Enlargement of the 1300–1370 cm^{-1} area illustrated in (**B**); (**D**) Figure of a single ZnO@ZIF-8 nanoparticle; (**E**,**F**) Figure of pNTP Raman detection at (**E**) below monolayer coverage and (**F**) over monolayer coverage concentrations. The EM (CM) enhanced pNTP peak is painted in orange (yellow); (**G**) UV-vis spectra of ZnO, ZIF-8, and ZnO@ZIF-8. Inset: Graph for the determination of band gap of ZnO@ZIF-8 $(Ahv)^2$ plotted against hv; (**H**) The energy level diagram illustrates the relative relationship between 4-cyanobenzoic acid and ZnO@ZIF-8; (**I**) Raman spectra of 4-cyanobenzoic acid molecules on ZIF-8, ZnO, and ZnO@ZIF-8.

Then, the UV-Vis spectroscopy was employed to characterize the light absorption properties of the synthesized ZnO@ZIF-8 materials. As demonstrated in Figure 2G, absorption peaks were observed at 230 nm for ZIF-8, ZnO, and ZnO@ZIF-8. In comparison with the single ZIF-8, the ZnO@ZIF-8 composite material presented a new absorption peak at 370 nm, and the characteristic peaks observed in the 300–400 nm range were due to the vibration of the metal-oxygen bond Zn=O of ZnO. Through the analysis of the Dow spectra obtained using the UV data (Figure 2G inset), the band gap of ZnO@ZIF-8 was calculated to be approximately 3.17 eV. It is universally known that SERS enhancement based on chemical mechanisms mainly depends on the energy level matching effect between the signal molecule and the substrate. However, in the ZnO@ZIF-8/4-cyanobenzoic acid system, since the LUMO value of 4-cyanobenzoic acid is higher than the CB of ZnO@ZIF-8 composite, the CT

process cannot occur (Figure 2H). Therefore, the chemical Raman enhancement of 4-cyanobenzoic acid on ZnO@ZIF-8 can be neglected. Next, the SERS performance of the ZnO@ZIF-8 composite material was tested using 4-cyanobenzoic acid as the probe molecule under the excitation of a 532 nm laser. As shown in Figure 2I, under 532 nm laser excitation, only when the 4-cyanobenzoic acid molecule is adsorbed on ZnO@ZIF-8 can a clear Raman signal be detected, while the Raman enhancement signal cannot be observed on the individual ZnO and ZIF-8 substrates.

Aiming to quantitatively evaluate the Raman signal enhancement effect of 4-cyanobenzoic acid on the ZnO@ZIF-8 composite material, we calculated its Raman intensity at 2232 cm^{-1} (the peak of -CN stretching vibration). The value of its enhancement factor (EF) was calculated to be approximately 5.3×10^4 [31,32]. The calculation results show that the ZnO@ZIF-8 substrate has a significant Raman signal enhancement effect on the 4-cyanobenzoic acid signal molecule, with an enhancement factor of up to 5.3×10^4, proving that this composite material has good SERS activity (for calculation details, refer to S18).

3.3. SERS Detection for P. gingivalis

In this project, we developed a well-performed SERS detection by making use of a DNA aptamer, which is composed of a specific sequence of DNA, and 4-cyanobenzoic acid as the signal molecule, in order to achieve the ultra-sensitive and selective detection of *P. gingivalis*. Compared with antibodies, aptamers exhibited superior stability over a wider range of temperature range and afforded more available binding sites [33]. As illustrated in Figure 3A, the ZnO@ZIF-8 composite was first experienced amination by 3-aminopropyltriethoxysilane (APTES), owing to its contribution of an amine functional group. Subsequently, the DNA aptamer of *P. gingivalis* with a carboxyl group at the 5′ end was added. Through the chemical reaction between the amino and the carboxyl group, generating an amide bond, the DNA aptamer was stably fixed on ZnO@ZIF-8 substrates. Then, the amino-modified complementary DNA (cDNA) loaded with a signaling molecule was stably bound to the surface of ZnO@ZIF-8 substrates through the reaction of DNA hybridization. Upon adding *P. gingivalis*, attributable to the great affinity between the aptamer and *P. gingivalis*, the cDNA conjugated with 4-cyanobenzoic acid split away from the surface of ZnO@ZIF-8 substrates. Thus, a distinct fall would be seen in the corresponding SERS signal. Therefore, highly selective and sensitive detection of *P. gingivalis* is achievable by using the SERS detection platform supported by ZnO@ZIF-8 substrates (for the build details of the SERS platform, refer to S11).

To assess the detection accuracy of *P. gingivalis* with the built SERS platform, we have prepared a series of groups containing various concentrations of *P. gingivalis*. As illustrated in Figure 3B,C, the signal levels at approximately 2232 cm^{-1}, which corresponds to 4-cyanobenzoic acid molecules, decreased with the increase in the concentration of *P. gingivalis*. The signal peak at 1455 cm^{-1} corresponding to ZnO@ZIF-8, by contrast, remained basically unchanged and consequently, was able to act as a reference signal to enhance reliability and veracity of the detection. Over a wide concentration range from 4×10^3 to 4×10^8 CFU/mL, the SERS intensity ratio of I_{2232}/I_{1455} demonstrated a great linear correlation ($R^2 = 0.9971$), attaining a limit of detection (LOD) as low as 38 CFU/mL (S19). The LOD based on this platform was lower than all the other common detection methods (Supplementary Materials Table S1). Moreover, the selectivity of the SERS detection platform was assessed under the conditions of all kinds of interfering compounds, containing *P. gingivalis*, Fusarium oxysporum, Treponema scaling, Actinobacterium actinomycetes, Pseudomonas aeruginosa, IL-1 β, IL-6, TNF-α, IL-17, MMP-8, MMP-9, LDH, AST, S100A8, CD9, CD81, TNF-β, CRP, citrullinated protein, gingival protease antibody BSA, DOPAC, UA, AA, CC, ADP, VA, ATP, His, Glu, and NE (Figure 3D). The intensity ratio of I_{2232}/I_{1455} for these interfering compounds remained constant as expected, since the combination of DNA aptamer and *P. gingivalis* did not interfere with other substances. In contrast, a notable decrease in the SERS intensity ratio of I_{2232}/I_{1455} was witness as a result of the presence of *P. gingivalis*. Furthermore, the ratiometric intensity ratio of the SERS signal (I_{2232}/I_{1455}) exhibited an intensity decline of more than 70% and reached its stable figure within 30 min, which revealed the ultrafast response of this detection platform (Figure 3E). Also, the platform presented a satisfactory long-term stability for 60 days (Figure 3F) with RSD = 8.532% (for calculation details, refer to S20), and an ideal repeatability (Figure 3G) with RSD = 1.476% (for calculation details, refer to S20), providing more possibility for the application in the detection of *P. gingivalis* in authentic clinical samples. Furthermore, as the environmental temperature and pH change, the signal intensity ratio (I_{2232}/I_{1455}) will fluctuate accordingly. However, the accuracy of the detection will not be affected under normal testing temperature and pH conditions (illustrated in S21 and S22).

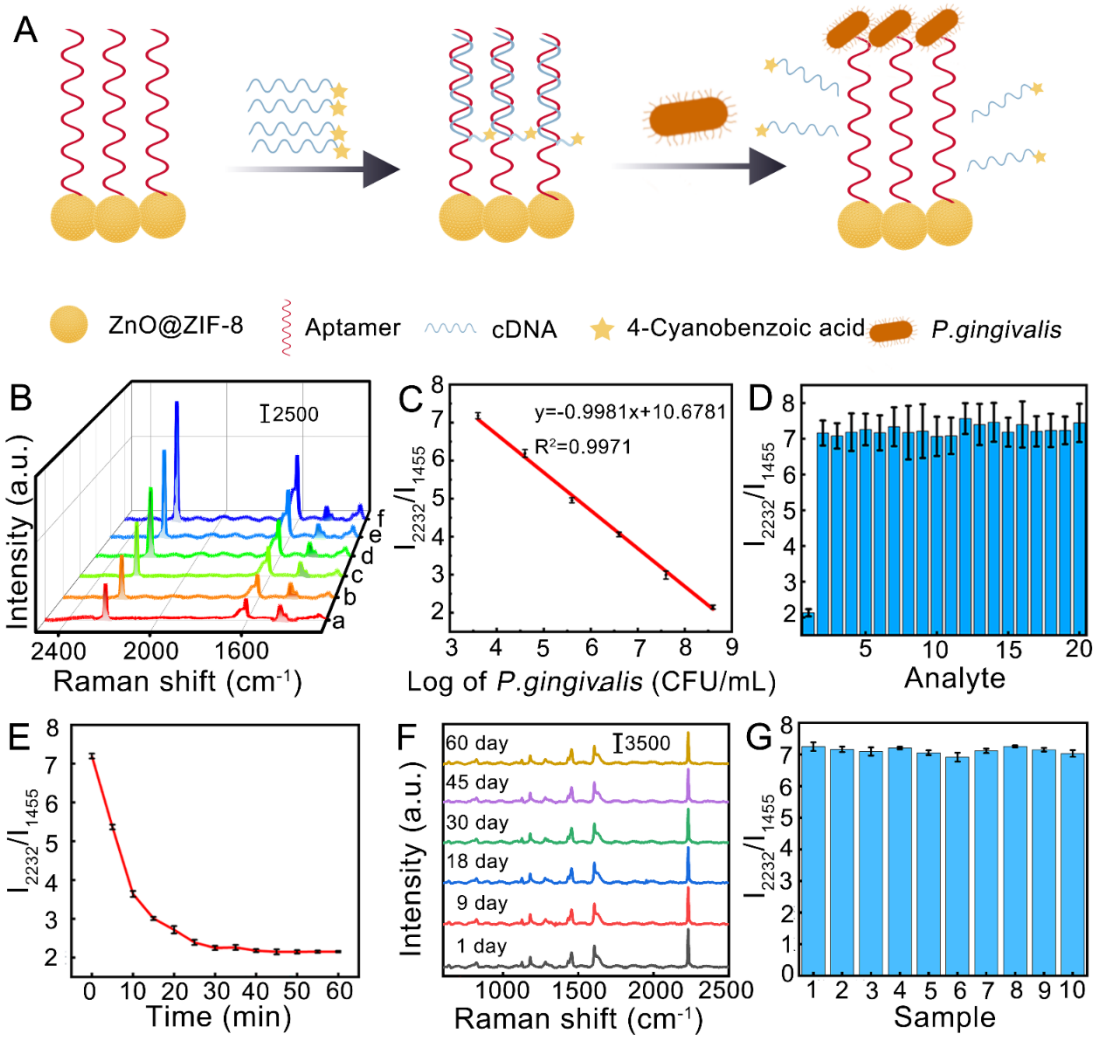

Figure 3. (**A**) Build based on ZnO@ZIF-8. The SERS platform is used for highly sensitive detection of *P. gingivalis* (Reprinted with permission from Ref. [34]. Copyright 2025, copyright Jian Ren et. al.); (**B**) Raman spectra of SERS platform at concentrations of (a) 4×10^8, (b) 4×10^7, (c) 4×10^6, (d) 4×10^5, (e) 4×10^4, and (f) 4×10^3 CFU/mL of *P. gingivalis*; (**C**) The relationship between SERS intensity ratio I_{2232}/I_{1455} and *P. gingivalis* concentration; (**D**) SERS monitoring of *P. gingivalis* for selective testing of other potential interferents (1–20, respectively: *P. gingivalis*, Fusarium oxysporum, Treponema scaling, Actinobacterium actinomycetes, Pseudomonas aeruginosa, IL-1 β, IL-6, TNF-α, IL-17, MMP-8, MMP-9, LDH, AST, S100A8, CD9, CD81, TNF-β, CRP, citrullinated protein, gingival protease antibody); (**E**) Response time of the SERS platform.

3.4. SERS Detection for P. gingivalis in Artificial Saliva

We further monitored the selectivity concerning *P. gingivalis* in simulated saliva of the SERS platform aimed to validate the applicability and suitability of it as a clinical diagnostic tool.

Firstly, we conducted the spike recovery experiment (S23), which excluded the influence of the artificial saliva solution on the detection of *P. gingivalis* using this SERS platform. After that, we utilized artificial saliva to simulate actual samples. A series of gradient dilutions based on the previous standard solution of *P. gingivalis* was conducted and used as the experimental group. The control group, on the other hand, replaced the solvent with artificial saliva to simulate the actual oral environment of the human body. Subsequently, both the experimental group and the control group were detected using the previously established ZnO@ZIF-8 SERS platform. The experimental results revealed that in artificial saliva, the concentration of *P. gingivalis* still could exhibit a similar figure as the experimental group within an error of 5% as shown in Figure 4B. These findings demonstrate that the designed SERS platform has favorable biological applicability for the determination of *P. gingivalis* content in the oral cavity.

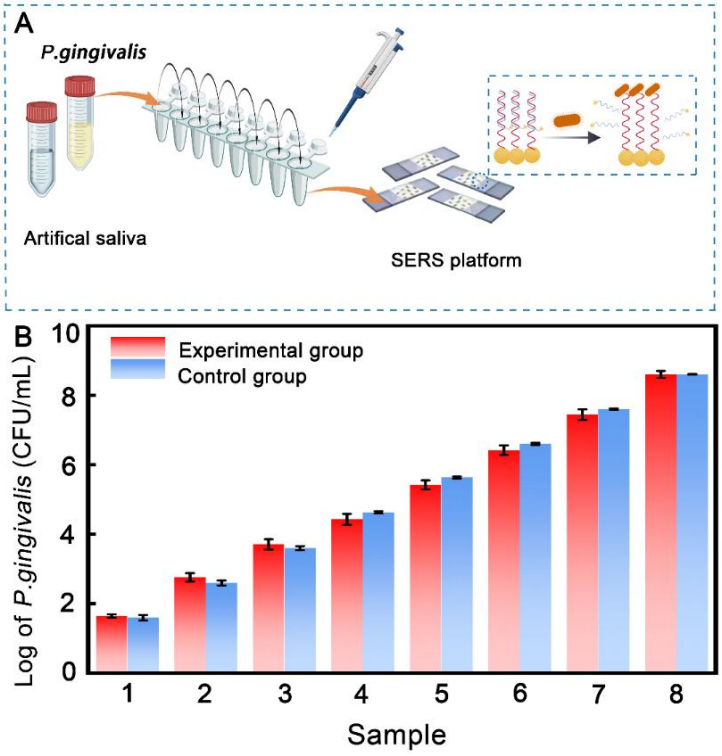

Figure 4. (**A**) The detection process regarding *P. gingivalis* in artificial saliva (Reprinted with permission from Ref. [34]. Copyright 2025, copyright Jian Ren et. al.); (**B**) Comparison of the stability for the built SERS platform between artificial saliva and the standard group.

4. Conclusions

To summarize, our work has developed a fast, ultrasensitive, and stable SERS platform for the detection of the main pathogenic microorganism for periodontitis, *P. gingivalis*, in saliva. Firstly, the petal-shaped spherical ZnO@ZIF-8 composite materials were prepared as the SERS platform substrates by in-situ synthesis. Then, based on the EM, it was calculated that the EF value of ZnO@ZIF-8 for the 4-cyanobenzoic acid signal molecule was up to 5.3×10^4. After that, the aptamer *of P. gingivalis* was assembled on the surface of the ZnO@ZIF-8 composite through amide bond formation, whereas the cDNA equipped with 4-cyanobenzoic acid was immobilized via the hybridization reaction. The SERS platform with high speed, excellent selectivity, and sensitivity, designed for the determination of *P. gingivalis*, was eventually fabricated. This platform, which has a quick detection speed in 30 min and a favourable stability for 60 days, demonstrated a wide linear range from 4×10^3 CFU/mL to 4×10^8 CFU/mL. Additionally, the LOD of this platform was calculated to be 38 CFU/mL, lower than other common detection methods for *P. gingivalis*. Furthermore, compared with standard samples in artificial saliva, this SERS platform revealed a superior stability for *P. gingivalis* detection. In summary, this rapid, sensitive, and stable SERS detection platform of *P. gingivalis* in saliva could make significant contributions to the improvement in preventive monitoring for periodontal disease. Also, in terms of the practical application aspects, this SERS platform has the advantages of a relatively simple preparation process, low cost of the synthesis of SERS substrates and the detection of *P. gingivalis*, and high scalability due to the substitutability of the aptamer and microorganisms. Therefore, this SERS platform has significant value and a promising application prospect. Overall, the SERS method developed in this work not only opens up a new research path for precise diagnosis and efficient screening of periodontal diseases, but also explores new directions for the detection of other disease-related proteins, small molecules, peptides, and miRNAs.

Supplementary Materials

The additional data and information can be downloaded at: https://media.sciltp.com/articles/others/25111214 49098477/NENP-25090136-Supplementary-Materials-FC-done.pdf. Figure S1: The Infrared spectra of ZnO@ZIF-8 and amino-modified ZnO@ZIF-8. Figure S2: The UV-Vis absorption spectra of (**i**) amino-modified ZnO@ZIF-8 complex with DNA aptamer and (**ii**) amino-modified ZnO@ZIF-8. Figure S3: The UV-Vis absorption spectra of (**i**) 4-cyanobenzoic acid complex with cDNA and (**ii**) 4-cyanobenzoic acid. Figure S4: The UV-Vis absorption spectra of (**i**) amino functionalized ZnO@ZIF-8 complex with DNA aptamer; (**ii**) complex with 4-cyanobenzoic acid and

cDNA; and (**iii**) SERS platform. Figure S5: SEM image of ZnO. Figure S6: SEM image of ZIF-8. Figure S7: The stability of the platform varies with temperature. Figure S8: The stability of the platform varies with pH. Table S1: Comparison of the common methods for *P. gingivalis* detection. Table S2: Comparison of the EF & LOD values for ZnO as different SERS substrates. References [35–43] are cited in the supplementary materials.

Author Contributions

X.Z., Z.L., and Q.L.: experimental operation, data analysis, and writing (original draft preparation); X.X.: references arrangement; T.Z.: project design, writing (reviewing and editing). All authors have read and agreed to the published version of the manuscript.

Funding

This research was funded by the National Natural Science Foundation of China (22222405 and 2024YFC3400125 for T. Zheng) and the East China Normal University Undergraduate Training Program on Innovation and Entrepreneurship grant 202510269163X.

Data Availability Statement

All data are available in the article and its Supplementary Information. Additional requests can be directed to the corresponding author.

Conflicts of Interest

The authors declare no conflict of interest.

Use of AI and AI-Assisted Technologies

No AI tools were utilized for this paper.

References

1. Xin, X.R.; Liu, J.J.; Liu, X.C.; et al. Melatonin-Derived Carbon Dots with Free Radical Scavenging Property for Effective Periodontitis Treatment via the Nrf2/HO-1 Pathway. *ACS Nano* **2024**, *18*, 8307–8324.
2. Huang, H.Y.; Pan, W.Y.; Wang, Y.F.; et al. Nanoparticulate Cell-free DNA Scavenger for Treating Inflammatory Bone Loss in Periodontitis. *Nat. Commun.* **2020**, *13*, 5925.
3. Ray, R.R. 2D MOF Periodontitis Photodynamic Ion Therapy. *J. Am. Chem. Soc.* **2021**, *143*, 15427–15439.
4. Hajishengallis, G. Periodontitis: From Microbial Immune Subversion to Systemic Inflammation. *Nat. Rev. Immunol.* **2015**, *15*, 30–44.
5. Potempa, J.; Mydel, P.; Koziel, J. The Case for Periodontitis in the Pathogenesis of Rheumatoid Arthritis. *Nat. Rev. Rheumatol.* **2017**, *13*, 606–620.
6. Nazir, M.; Al-Ansari, A.; Al-Khalifa, K.; et al. Global Prevalence of Periodontal Disease and Lack of Its Surveillance. *Sci. World J.* **2020**, 2146160. https://doi.org/10.1155/2020/2146160.
7. Jia, L.; Jiang, Y.Y.; Wu, L.L.; et al. *Porphyromonas gingivalis* Aggravates Colitis Via a Gut Microbiota-linoleic Acid Metabolism-Th17/Treg Cell Balance Axis. *Nat. Commun.* **2024**, *15*, 1617.
8. Sands, K.; Carvalho, M.J.; Portal, E.; et al. Characterization of Antimicrobial-resistant Gram-negative Bacteria that Cause Neonatal Sepsis in Seven Low-and middle-income Countries. *Nat. Microbiol.* **2021**, *6*, 512–532.
9. Murugaiyan, V.; Utreja, S.; Hovey, K.M.; et al. Defining *Porphyromonas gingivalis* Strains Associated with Periodontal Disease. *Sci. Rep*. **2024**, *14*, 6222.
10. Quick, J.; Grubaugh, N.D.; Pullan, S.T.; et al. Multiplex PCR Method for MinION and Illumina Sequencing of Zika and Other Virus Genomes Directly from Clinical Samples. *Nat. Protoc.* **2021**, *25*, 266–271.
11. Weng, Z.Y.; You, Z.; Yang, J.; et al. CRISPR-Cas Biochemistry and CRISPR-Based Molecular Diagnostics. *Angew. Chem. Int. Ed.* **2023**, *62*, e202214987.
12. Smyrlaki, I.; Ekman, M.; Lentini, A.; et al. Massive and Rapid COVID-19 Testing is Feasible by Extraction-free SARS-CoV-2 RT-PCR. *Nat. Commun.* **2020**, *11*, 4812.
13. Qian, X.M.; Nie, S.M. Single-molecule and Single-nanoparticle SERS: From Fundamental Mechanisms to Biomedical Applications. *Chem. Soc. Rev.* **2008**, *37*, 912–920.
14. Su, X.M.; Liu, X.Y.; Ouyang, Y.Z.; et al. SERS Lateral Flow Strip Detection of Serum Biomarkers for Noninvasive Assessment of Operative Microwave Ablation Outcomes of Unresectable Hepatocellular Carcinoma. *Chem. Eng. J.* **2024**, *485*, 149833.

15. Shin, H.; Choi, B.H.; Shim, O.; et al. Single Test-based Diagnosis of Multiple Cancer Types Using Exosome-SERS-AI for Early Stage Cancers. *Nat. Commun.* **2024**, *14*, 1644.
16. Bi, X.Y.; Daniel, M.C.; Shao, Z.F.; et al. Digital Colloid-enhanced Raman Spectroscopy by Single-molecule Counting. *Nature* **2024**, *628*, 771–775.
17. Evelin, W.; Anna, M.L.; Krzysztof, N.; et al. In Search of Spectroscopic Signatures of Periodontitis: A SERS-Based Magnetomicrofluidic Sensor for Detection of *Porphyromonas gingivalis* and *Aggregatibacter actinomycetemcomitans*. *ACS Sens.* **2021**, *6*, 1621–1635.
18. Prince, K.J.; Mirletz, H.M.; Gaulding, E.A.; et al. Sustainability Pathways for Perovskite Photovoltaics. *Nat. Mater.* **2025**, *24*, 22–33.
19. Song, G.; Gong, W.B.; Cong, S.; et al. Ultrathin Two-Dimensional Nanostructures: Surface Defects for Morphology-Driven Enhanced Semiconductor SERS. *Angew. Chem. Int. Ed.* **2021**, *60*, 5505–5511.
20. Han, S.W.; Han, H.S.; Kim, K. Potassium Ion Assisted Regeneration of Active Cyano Groups in Carbon Nitride Nanoribbons: Visible Light Driven Photocatalytic Nitrogen Reduction. *Angew. Chem. Int. Ed.* **2019**, *58*, 16644–16650.
21. Wang, Y.G.; Zhou, K.J.; Huang, G.; et al. A Nanoparticle-based Strategy for the Imaging of a Broad Range of Tumours by Nonlinear Amplification of Microenvironment signals. *Nat. Mater.* **2014**, *13*, 204–212.
22. Liu, X.Y.; Ye, Z.W.; Xiang, Q.; et al. Boosting Electromagnetic Enhancement for Detection of Non-adsorbing Analytes on Semiconductor SERS Substrates. *Chem* **2023**, *9*, 1464–1476.
23. Tuncel, D.; Ökte, A.N. Improved Adsorption Capacity and Photoactivity of ZnO-ZIF-8 Nanocomposites. *Catal. Today* **2021**, *361*, 191–197.
24. Liang, W.L.; Cheng, J.L.; Zhang, J.D.; et al. pH-Responsive On-Demand Alkaloids Release from Core-Shell ZnO@ZIF-8 Nanosphere for Synergistic Control of Bacterial Wilt Disease. *ACS Nano* **2022**, *16*, 2762–2773.
25. Liang, W.L.; Wang, B.; Cheng, J.L.; et al. 3D, Eco-Friendly Metal-Organic Frameworks@carbon Nanotube Aerogels Composite Materials for Removal of Pesticides in Water. *J. Hazard. Mater.* **2021**, *401*, 123718.
26. Jiang, S.Q.; Li, W.D.; Liu, J.Y.; et al. ZnO@ZIF-8 Core-shell Structure Nanorods Superhydrophobic Coating on Magnesium Alloy with Corrosion Resistance and Self-cleaning. *J. Magnes. Alloys* **2023**, *11*, 3287–3301.
27. Lai, Y.J.; Dong, L.J.; Liu, R.; et al. Synthesis of Highly-branched Au@AgPd Core/shell Nanoflowers for in situ SERS Monitoring of Catalytic Reactions. *Chin. Chem. Lett.* **2020**, *31*, 2437–2441.
28. Li, S.K.; Li, Z.Y.; Hao, Q.; et al. Ultrastable Graphene Isolated AuAg Nanoalloy for SERS Biosensing and Photothermal Therapy of Bacterial Infection. *Chin. Chem. Lett.* **2024**, *35*, 108636.
29. Quan, Y.N.; Tang, X.H.; Lu, W.J.; et al. Amorphous/Crystal Heterostructure Coupled Oxygen Vacancies-Sensitized TiO_2 with Conspicuous Charge-Transfer Resonance for Efficient Sers Detection of Chloramphenicol. *Adv. Opt. Mater.* **2023**, *11*, 2301609.
30. Xu, Y.C.; Li, C.L.; Li, Z.Q.; et al. Constructing Charge-Transfer Excited States Based on Frontier Molecular Orbital Engineering: Narrowband Green Electroluminescence with High Color Purity and Efficiency. *Angew. Chem. Int. Ed.* **2020**, *59*, 17442–17446.
31. Cheng, H.; Chen, R.J.; Zhan, Y.Q.; et al. Novel Ratiometric Surface-Enhanced Raman Scattering (SERS) Biosensor for Ultrasensitive Quantitative Monitoring of Human Carboxylesterase-1 in Hepatocellular Carcinoma Cells Using Ag-Au Nanoflowers as SERS Substrate. *Anal. Chem.* **2024**, *96*, 18555–18563.
32. Sibug-Torres, S.M.; Grys, D.B.; Kang, G.; et al. *In Situ* Electrochemical Regeneration of Nanogap Hotspots for Continuously Reusable Ultrathin SERS Sensors. *Nat. Commun.* **2024**, *15*, 2022.
33. Lin, X.M.; Sun, Y.L.; Chen, Y.X.; et al. Insights into Electrocatalysis through in situ Electrochemical Surface-enhanced Raman Spectroscopy. *eScience* **2024**, *7*, 100352.
34. Jiang, S.; Li, H.; Zhang, L.; et al. Generic Diagramming Platform (GDP): A comprehensive database of high-quality biomedical graphics. *NAR* **2025**, *53*, 1670–1676.
35. Ji, W.; Li, L.; Song, W.; et al. Enhanced Raman Scattering by ZnO Superstructures: Synergistic Effect of Charge Transfer and Mie Resonances. *Angew. Chem. Int. Ed.* **2019**, *58*, 14452–14456.
36. Wang, W.; Deng, C.; Xie, S.; et al. Photocatalytic C-C Coupling from Carbon Dioxide Reduction on Copper Oxide with Mixed-valence Copper(I)/Copper(II). *J. Am. Chem. Soc.* **2021**, *143*, 2984–2993.
37. Gomes, B.P.F.A.; Pinheiro, E.T.; Gadê-Neto, C.R.; et al. Microbiological Examination of Infected Dental Root Canals. *Mol. Oral Microbiol.* **2004**, *19*, 71–76.
38. Gu, B.L.; Qi, Y.J.; Kong, J.Y.; et al. An Evaluation of Direct PCR Assays for the Detection and Quantification of *P. gingivalis*. *Epidemiol. Infect.* **2020**, *148*, e107.
39. Ingalagi, P.; Bhat, K.G.; Kulkarni, R.D.; et al. Detection and Comparison of Prevalence of *Porphyromonas gingivalis* through Culture and Real Time-polymerase Chain Reaction in Subgingival Plaque Samples of Chronic Periodontitis and Healthy Individuals. *J. Oral Maxillofac. Pathol.* **2022**, *26*, 288.

40. Su, Y.X.; Huang, S.M.; Hong, L.; et al. Establishment of the Molecular Beacon-loop-mediated Isothermal Amplification Method for the Rapid Detection of *P. gingivalis*. *J. Microbiol. Methods* **2019**, *160*, 68–72.
41. Shin, H.Y.; Shim, E.L.; Choi, Y.J.; et al. Giant enhancement of the Raman response due to one-dimensional ZnO nanostructures. *Nanoscale* **2014**, *6*, 14622–14626.
42. Wang, Y.; Ruan, W.; Zhang, J.; et al. Direct observation of surface-enhanced Raman scattering in ZnO nanocrystals. *J. Raman Spectrosc.* **2009**, *40*, 1072–1077.
43. Luo, Y.W.; Niu, L.Y.; Wang, Y.F.; et al. Experimental and theoretical evaluation of crystal facet exposure on the charge transfer and SERS activity of ZnO films. *Nanoscale* **2022**, *14*, 16220–16232.